

Hydrodynamics of sediment transport: grain scale to continuum scale

Subhasish Dey & Sk Zeeshan Ali

Department of Civil Engineering, Indian Institute of Technology Kharagpur, West Bengal 721302, India

ABSTRACT: A theory of sediment transport, describing the entrainment phenomenon from the grain scale to the continuum scale, under a steady-uniform flow over a sediment bed is presented. The sediment grains, assumed as discrete spherical grains, are subjected to turbulent wall-shear flows. At the grain scale, the forces acting on a sediment grain resting over three compact spherical grains are analysed to determine the criteria for entrainment threshold in rolling, sliding and lifting modes taking into account the turbulence effects. Comparison of the theoretical results with the experimental data shows that the entrainment threshold lies within the sliding and lifting modes. Then, at the grain scale, using the log-normal probability density function for the near-bed instantaneous horizontal velocity, the entrainment probabilities in rolling, sliding and lifting modes for a given grain size are derived. The rolling and sliding probabilities increase with an increase in Shields function and after attaining their individual maximum values, they reduce, whereas the lifting probability increases with Shields function. The maximum value of entrainment probability in rolling mode is close to the threshold Shields function in rough flow, whereas the entrainment probability in lifting mode initiates from the value of the threshold Shields function. In a continuum scale, the bedload flux is derived by hypothesising the saltating mode of sediment transport incorporating the lifting probability obtained at the grain scale.

1 GENERAL

When the stream flows over a sediment bed, the hydrodynamic drag and lift forces act on the sediment grains at the bed surface. As the stream velocity enhances, a state is ultimately reached when the sediment grains at the bed surface are entrained intermittently if the hydrodynamic forces overcome the stabilising force arising from the submerged weight of the sediment grains, called the *entrainment threshold of sediment*. Different feasible modes of entrainment threshold of sediment are rolling, sliding and lifting modes, as depicted schematically in Figure 1. In rolling mode, the overturning moment on the sediment grain about the pivot point exceeds the stabilising moment about that point, whereas in sliding mode, the drag force on the sediment grain exceeds the frictional resistance at the contacts of the grains. On the other hand, in lifting mode, the lift force exceeds the submerged weight of the sediment grain. The complexity of the interaction between the sediment grains and the turbulent flow renders the problem of sediment transport intricate. Thus, the complex phenomenon impedes to achieve a comprehensive theoretical analysis. Regarding the applications of the knowledge of sediment transport, it plays an important role in analysing the stability and ex-

tending the lifetime of important riverine structures, such as bridge, barrage, culvert, reservoir dam, etc.

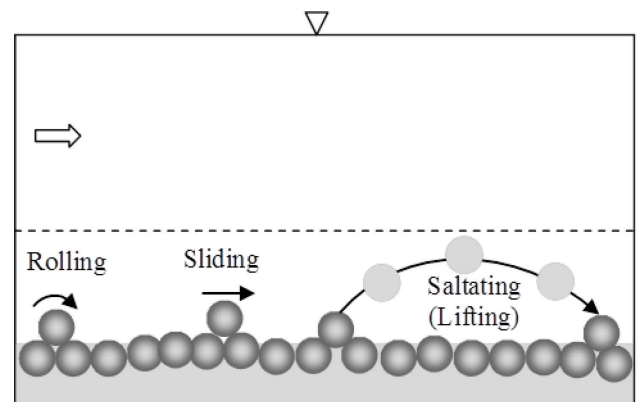


Figure 1. Schematic of bedload transport with the motion of sediment grains in rolling, sliding and saltating (or lifting) modes.

The study on entrainment threshold of sediment by the streamflow was pioneered by Shields (1936). He did a semi-theoretical analysis to recommend the famous *Shields diagram*. His diagram represents a curve (well-known as *Shields curve*) of threshold Shields function Θ_c versus shear Reynolds number R_* and is commonly used to determine the threshold bed shear stress for a given median size of sediment

grain. Later, experimental observations of Fenton & Abbott (1977) indicated that the threshold bed shear stress has a dependence on the exposure of sediment grains to the flow. As a consequence, a slight deviation of the Shields curve from the experimental data band in the hydraulically smooth and rough flows was reported (Mantz, 1977; Miller et al., 1977; Yalin & Karahan, 1979). Since then many researchers contributed experimentally and theoretically to the topic of entrainment threshold of sediment. Comprehensive review on the topic of entrainment threshold of sediment was done by Miller et al. (1977), Buffington & Montgomery (1997), Garcia (2008) and Dey (2014).

When the bed shear stress induced by the flow slightly exceeds its critical value for the entrainment threshold of sediment, the sediment grains begin to entrain in *rolling* or *sliding modes*, but not detached from the bed. With an additional increase in bed shear stress, the sediment grains are momentarily lifted performing series of brief jumps along the bed remaining confined to the bedload layer, termed *saltating* or *lifting mode*. The transport of sediment grains in rolling, sliding and saltating or lifting modes is called *bedload transport* of sediment (Fig. 1). Einstein (1942, 1950) and Bagnold (1956) hypothesised that the mode of bedload transport is saltating mode, which was afterward experimentally verified by Francis (1973) and Abbott & Francis (1977). It is distinctive that the lift force basically governs the saltation of sediment grains. Einstein (1950), in his famous theory of the bedload transport, hypothesised the sediment entrainment phenomenon from the viewpoint of the probability of instantaneous lift force generated by the velocity fluctuations exceeding the submerged weight of the sediment grains. The probabilistic notion of sediment entrainment is an essential criterion to analyse the sediment entrainment phenomenon, because the highly intermittent near-bed turbulence intermingles with the sediment grains to play an important role in transporting them (Cheng & Chiew, 1998; Papanicolaou et al., 2001, 2002; Wu & Lin, 2002; Wu & Chow 2003; Zanke, 2003; Wu & Yang, 2004; Dey et al., 2011, 2012; Tregnaghi et al., 2012). Interestingly, the turbulent bursting phenomenon in turbulent flow (Kline et al., 1967), after its discovery, has created a new look to further explore the sediment entrainment phenomenon. In turbulent bursting, the conditional Reynolds shear stresses have a substantial departure from the time-averaged Reynolds shear stress during the intermittent events. Consequently, such events have a strong contribution towards the sediment entrainment phenomenon (Sutherland, 1967; Heathershaw & Thorne, 1985; Wu & Jiang 2007; Dey et al., 2011, 2012). The ejections and sweeps, amongst the bursting events, are the most pertinent events towards the entrainment process because they produce a positive input to the Reynolds

shear stress. Nevertheless, a number of authors argued that the Reynolds shear stress is not the most relevant contributor to govern the entrainment process and to transport the sediment grains (Williams et al., 1989; Clifford et al., 1991; Papanicolaou et al., 2001, 2002; Schmeckle & Nelson, 2003). They identified that the entrainment threshold of sediment grains and the bedload transport are much linked with the instantaneous horizontal velocity.

In spite of significant advancement made to establish the probabilistic theory of sediment entrainment (Cheng & Chiew, 1998; Papanicolaou et al., 2002; Wu & Lin, 2002; Wu & Chow, 2003; Wu & Yang, 2004; Wu & Jiang, 2007; Tregnaghi et al., 2012), a comprehensive analysis of the force system in a three-dimensional configuration of the bed sediment grains, as a probabilistic-cum-micromechanical aspect, seems to have received little attention. Moreover, most of the existing analyses are based on a single velocity law of the wall (logarithmic law) for the hydraulically rough-turbulent flow and a single value of the horizontal turbulence intensity near the bed. Further, no probabilistic theory describing the entrainment phenomenon of sediment was extended from the grain scale to the continuum scale.

This study presents a theory of sediment transport from the grain scale of entrainment to the continuum scale of bedload flux for a steady-uniform flow over a sediment bed considering a three-dimensional configuration of the granular bed of sediment. At the grain scale, the hydrodynamic drag and lift forces acting on a solitary sediment grain (spherical) are analysed considering velocity laws for the hydraulically smooth, transitional and rough flows. The forces are analysed to examine the entrainment threshold in rolling, sliding and lifting modes introducing the turbulence effects. A probabilistic analysis of sediment entrainment is done using the log-normal probability density function for the near-bed instantaneous horizontal velocity. The entrainment probabilities for the rolling, sliding and lifting modes are obtained for a given median size of grains. Finally, the bedload flux, as a continuum scale, is analysed by using the entrainment probability in lifting mode.

2 SEDIMENT ENTRAINMENT AT GRAIN SCALE

2.1 *Mechanics of sediment entrainment*

At the grain scale, a spherical solitary or target sediment grain of diameter D , resting over a compact granular sediment bed formed by the similar sediment grains of diameter d is shown in Figure 2. A tetrahedron $CC_1C_2C_3$ is formed joining the centres of the solitary sediment grain and the bed sediment grains by the straight lines. Figure 3 illustrates the enlarged view of the tetrahedron. The points of con-

tact of the solitary sediment grain with the three bed sediment grains are G_1 , G_2 and G_3 . The imaginary bed level, fixing $z = 0$, is assumed at a vertical distance ξd below the crest level of the bed sediment grains (Fig. 2), where ξ is a factor being less than unity. The vertical distance of the lowest point of the solitary sediment grain from the imaginary bed level is given by $\delta = \xi d - 0.5(D + d) + CJ$. From the three-dimensional geometry, the length CJ is obtained as

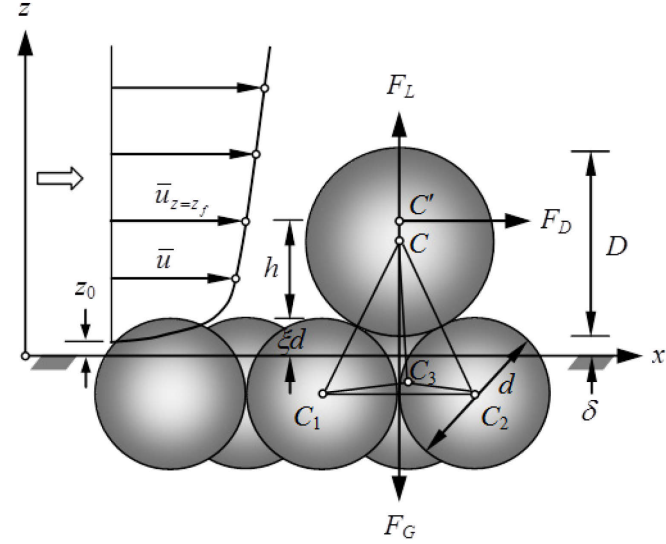


Figure 2. Typical three-dimensional configuration of bed sediment grains and the force system.

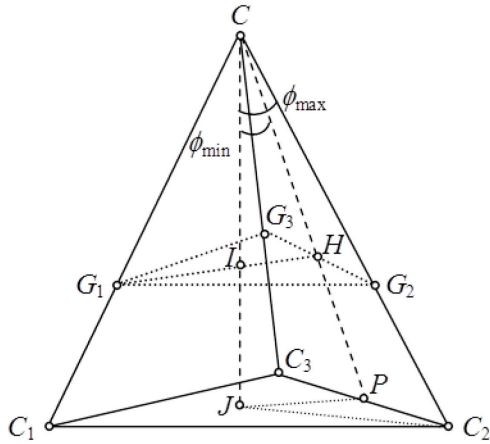


Figure 3. Tetrahedron formed joining the centres of the solitary sediment grain and the bed sediment grains by the straight lines.

$$CJ = (CC_2^2 - C_2J^2)^{0.5} = \left[\left(\frac{D+d}{2} \right)^2 - \left(\frac{d}{\sqrt{3}} \right)^2 \right]^{0.5}$$

$$= \frac{1}{2\sqrt{3}} (3D^2 + 6Dd - d^2)^{0.5} \quad (1)$$

Then, the $\hat{\delta}$ ($= \delta/D$) is given by

$$\hat{\delta} = \xi \hat{d} - 0.5(1 + \hat{d}) + \frac{1}{2\sqrt{3}} (3 + 6\hat{d} - \hat{d}^2)^{0.5} \quad (2)$$

where $\hat{d} = d/D$.

In rolling mode, the solitary sediment grain can entrain rolling either over the crest of a single bed sediment grain or over the cusp formed by the two neighbouring bed sediment grains. In the former event, the solitary sediment grain rolls towards JC_2 and the pivot angle ϕ attains its maximum value ϕ_{max} (Fig. 3). In the latter event, the solitary sediment grain rolls towards JP and the pivot angle becomes a minimum ϕ_{min} (Fig. 3). From the three-dimensional geometry, the following relationships are obtained:

$$\tan \phi_{max} = \frac{C_2J}{CJ} = \frac{2\hat{d}}{(3 + 6\hat{d} - \hat{d}^2)^{0.5}} \quad (3)$$

$$\tan \phi_{min} = \frac{JP}{CJ} = \frac{\hat{d}}{(3 + 6\hat{d} - \hat{d}^2)^{0.5}} \quad (4)$$

The most possible way (as an average) to entrain the solitary sediment grain in a rolling mode is the midstream between the lengths JC_2 and JP . Since $\tan \phi_{max} = 2 \tan \phi_{min}$, for the average value of the pivot angle, $\tan \phi = 0.5(\tan \phi_{min} + \tan \phi_{max}) = 1.5 \tan \phi_{min}$ (Miller & Byrne, 1966). Thus, the ϕ is obtained as

$$\phi = \tan^{-1} \left[\frac{1.5\hat{d}}{(3 + 6\hat{d} - \hat{d}^2)^{0.5}} \right] \quad (5)$$

The hydrodynamic force acting on the solitary sediment grain is resolved into drag force F_D (acting flow direction) and lift force F_L (acting normal to the flow direction). Besides, the submerged weight F_G of the grain acts vertically downward. The force system is shown in Figure 2. The submerged weight is given by

$$F_G = \frac{\pi}{6} D^3 \Delta \rho_f g \quad (6)$$

where Δ = submerged relative density of sediment grains [$= (\rho_p - \rho_f)/\rho_f$]; ρ_f = mass density of fluid; ρ_p = mass density of sediment grains; and g = acceleration due to gravity.

In turbulent flow, the local instantaneous horizontal velocity $u(z)$ is decomposed as $u = \bar{u} + u'$, where \bar{u} is the time-averaged value of u and u' is the fluctuations of u with respect to \bar{u} . The instantaneous drag force acting at $z = z_f$ is

$$F_D = 0.5 C_D \rho_f u_{z=z_f}^2 A_f \quad (7)$$

where C_D = drag coefficient; $\bar{u}_{z=z_f}$ = instantaneous horizontal velocity at $z = z_f$, $z_f = \xi d + h$; h = vertical distance of the point of action of drag force from the crest level of the bed sediment grains; and A_f = frontal projected area of the spherical solitary sediment grain exposed to the flow. Morsi & Alexander (1972) reported $C_D = A_1 + A_2 R^{-1} + A_3 R^{-2}$, where R

$= \bar{u}_{z=z_f} D/\nu$; ν = coefficient of kinematic viscosity of fluid; and A_1 , A_2 and A_3 = coefficients dependent on R . In this study, this expression of C_D is used. The h is expressed as

$$h = \frac{\int_{\xi d}^{D+\delta} \bar{u}^2 z dA}{\int_{\xi d}^{D+\delta} \bar{u}^2 dA} \quad (8)$$

where dA = area of the horizontal strip across the frontal projection of the solitary sediment grain at $z = z$. It is expressed as $dA = 2[(z - \delta)(\delta + D - z)]^{0.5} dz$. Then, the \hat{z}_f ($= z_f/D$) is expressed as

$$\hat{z}_f = \xi \hat{d} + \frac{\int_{\xi \hat{d}}^{1+\hat{\delta}} u^{+2} \hat{z} [(\hat{z} - \hat{\delta})(1 + \hat{\delta} - \hat{z})]^{0.5} d\hat{z}}{\int_{\xi \hat{d}}^{1+\hat{\delta}} u^{+2} [(\hat{z} - \hat{\delta})(1 + \hat{\delta} - \hat{z})]^{0.5} d\hat{z}} \quad (9)$$

where $u^+ = \bar{u}/u_*$; u_* = shear velocity; and $\hat{z} = z/D$. The frontal projected area A_f of the spherical solitary sediment grain exposed to the flow is the circular projected area of the sphere above an imaginary plane at an elevation $z = \xi d$. Note that the crests of the bed sediment grains upstream of the solitary sediment grain intrude into the flow area beneath that imaginary plane. The \hat{A}_f ($= A_f/D^2$) is expressed as

$$\hat{A}_f = 0.25D^2 \{ \pi - \cos^{-1}(1 + 2\hat{\delta} - 2\xi \hat{d}) + 2(1 + 2\hat{\delta} - 2\xi \hat{d})[(1 + \hat{\delta} - \xi \hat{d})(\xi \hat{d} - \hat{\delta})]^{0.5} \} \quad (10)$$

The instantaneous lift force acting through the centre of the solitary sediment grain is

$$F_L = 0.5C_L \rho_f u_{z=z_f}^2 A_f \quad (11)$$

where C_L = lift coefficient. In this study, the value of $C_L = 0.2$ is assumed, as was considered by Wiberg & Smith (1987).

When the solitary sediment grain is about to roll, the moment balance of the force system about the pivot point therefore satisfies the criterion (Fig. 4a): $M_O \geq M_S$ yielding $F_L L_x + F_D L_z \geq F_G L_x$, where M_O = overturning moment; M_S = stabilizing moment; L_x = horizontal moment arm; and L_z = vertical moment arm. Substituting Equations 6, 7 and 11 into the criterion in rolling mode yields

$$u_{z=z_f}^2 \geq \Xi_R^2 = \frac{\pi D^3 \Delta g L_x}{3A_f (C_D L_z + C_L L_x)} \quad (12)$$

where Ξ_R = rolling threshold.

In sliding mode, the instantaneous drag force exceeds the frictional resistance at the contacts of the solitary sediment grain and the bed sediment grain. The horizontal force balance therefore provides the

criterion (Fig. 4b): $F_D \geq F_R$ yielding $F_D \geq (F_G - F_L) \tan \phi$. Substituting Equations 6, 7 and 11 into the criterion of sliding mode yields

$$u_{z=z_f}^2 \geq \Xi_S^2 = \frac{\pi D^3 \Delta g \tan \phi}{3A_f (C_D + C_L \tan \phi)} \quad (13)$$

where Ξ_S is the sliding threshold.

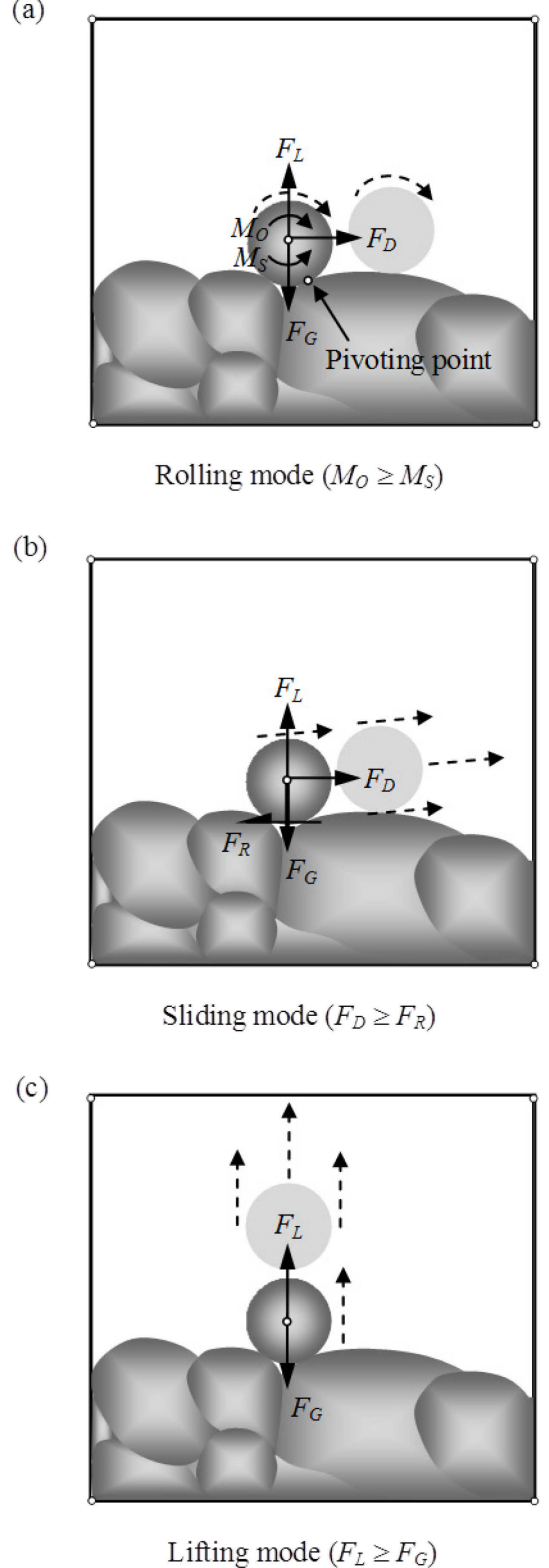


Figure 4. Schematic of different modes of sediment entrainment: (a) Rolling mode; (b) sliding mode; and (c) lifting mode.

In lifting mode, the instantaneous lift force exceeds the submerged weight of the solitary sediment grain. The vertical force balance thus yields the criterion (Fig. 4c): $F_L \geq F_G$. Substituting Equations 6, 7 and 11 into the criterion of lifting mode yields

$$u_{z=z_f}^2 \geq \Xi_L^2 = \frac{\pi D^3 \Delta g}{3A_f C_L} \quad (14)$$

where Ξ_L = lifting threshold.

From a close examination of Equations 12–14, it is distinguishable that the entrainment threshold has a kind of sequence in different modes as $\Xi_L > \Xi_S > \Xi_R$. Therefore, in case of $\Xi_R < u_{z=z_f} < \Xi_S$, the grains entrain only in a rolling mode touching the bed. On the other hand, in case of $\Xi_S < u_{z=z_f} < \Xi_L$, the grains entrain as a combination of rolling and sliding modes, while in case of $u_{z=z_f} > \Xi_L$, the grains entrain simultaneously in rolling and lifting modes. Thus, time-averaging of Equations 12–14, yields the threshold Shields functions in rolling, sliding and lifting modes:

$$\Theta_c(\text{rolling}) = \frac{\pi D^2 L_x}{3A_f (C_D L_z + C_L L_x)} \cdot \frac{u_*^2}{(\bar{u}^2 + \sigma_u^2)_{z=z_f}} \quad (15)$$

$$\Theta_c(\text{sliding}) = \frac{\pi D^2 \tan \phi}{3A_f (C_D + C_L \tan \phi)} \cdot \frac{u_*^2}{(\bar{u}^2 + \sigma_u^2)_{z=z_f}} \quad (16)$$

$$\Theta_c(\text{lifting}) = \frac{\pi D^2}{3A_f C_L} \cdot \frac{u_*^2}{(\bar{u}^2 + \sigma_u^2)_{z=z_f}} \quad (17)$$

where Θ = Shields function [= $u_*^2 / (\Delta g D)$]; σ_u = horizontal turbulence intensity [= $(u'u')^{0.5}$]; and subscript c represents the threshold criterion.

For any orientation of the bed sediment grains with respect to the flow direction, the moments of the forces F_D , F_L and F_G are taken in between about the pivot point G_1 (in case, the grain rolls over the crest of a single sediment grain) and the pivot line G_2G_3 (in case, the grain rolls over the cusp of the two neighbouring sediment grains) (Figs. 2 and 3). In a fluvial streambed, there are numerous orientations of the bed sediment grains within the aforementioned limits. The horizontal moment arm L_x for any orientation lies $G_1I \leq L_x \leq HI$. Thus, the L_x is approximated as an average $L_x = 0.5(G_1I + HI)$. From the geometry (Fig. 3), $G_1I = 0.5D \sin \phi_{\max}$ and $HI = 0.25D \sin \phi_{\max}$. Therefore, the \hat{L}_x (= L_x/D) in nondimensional form is given by

$$\hat{L}_x = 0.375 \sin \phi_{\max} \quad (18)$$

The vertical moment arm is obtained as $L_z = C'I = z_f - \delta - 0.5D(1 - \cos \phi_{\max})$. Therefore, the \hat{L}_z (= L_z/D) in nondimensional form is given by

$$\hat{L}_z = \hat{z}_f - \hat{\delta} - 0.5(1 - \cos \phi_{\max}) \quad (19)$$

The threshold Shields functions in rolling, sliding and lifting modes depend on the velocity laws in hydraulically smooth, transitional and rough flows, which are classified by the values of shear Reynolds number R^* ($= u_* k_s / \nu$, where k_s = Nikuradse's equivalent roughness) (Dey, 2014). In transitional flow ($3 < R^* < 70$), the velocity law proposed by Reichardt (1951) is used in this study. It is

$$u^+ = \frac{1}{\kappa} \left\{ \ln(1 + \kappa z^+ R^*) - \left[1 - \exp\left(-\frac{z^+ R^*}{11.6}\right) - \frac{z^+ R^*}{11.6} \exp\left(-\frac{z^+ R^*}{3}\right) \right] \ln(\kappa z_0^+ R^*) \right\} \quad (20)$$

where κ = von Kármán constant; $z^+ = z/k_s$; $z_0^+ = z_0/k_s$; and z_0 = zero-velocity level. Equation 20 has a flexibility, because it serves reasonably well estimates over a certain range of smooth ($R^* < 3$) flow. Therefore, in this study, Equation 20 is also used as the velocity law for the smooth flow ($0.1 \leq R^* < 3$).

For hydraulically rough flow ($R^* \geq 70$), the logarithmic law is used as the velocity law. It is

$$u^+ = \frac{1}{\kappa} \ln\left(\frac{z^+}{z_0^+}\right) \quad (21)$$

For the rough flow, $z_0^+ = 0.03$.

In case of weakly mobile beds, Dey et al. (2012) reported the average values of $z_0 = 0.04k_s$ and $\xi = 0.21$ and Best et al. (1997) suggested an average value of $\kappa = 0.385$. These values are used in this study.

Nezu (1977) proposed an expression for horizontal turbulence intensity σ_u , which is in nondimensional form σ_u^+ ($= \sigma_u/u_*$) given by

$$\sigma_u^+ = 2.3\Gamma \exp(-z^+) + 0.31(1 - \Gamma)z^+ R^* \quad (22)$$

where Γ = van Driest damping function = $[1 - \exp(-z^+ R^*/D_f)]$; and D_f = damping factor, which can be approximated as 10 (Nezu, 1977).

2.2 Probabilistic concept of sediment entrainment

The sediment entrainment is governed by the near-bed turbulence characteristics and hence the probability of the near-bed instantaneous velocity at the level of the solitary sediment grain relative to the bed sediment grains and their orientations with respect to the flow direction. Wu & Lin (2002) argued that the near-bed instantaneous horizontal velocity is expected to follow the log-normal distribution because the positive horizontal velocity fluctuations in the vicinity of the bed are main mechanism towards the sediment entrainment. Symbolising $v = \ln u$, the probability density function f_v of $v_{z=z_f}$ is expressed as

$$f_v[v_{z=z_f} \in (0, \infty)] = \frac{1}{\sqrt{2\pi} \sigma_v|_{z=z_f}} \exp\left[-\frac{(v-\bar{v})^2}{2\sigma_v^2}\right]_{z=z_f},$$

$$f_v[v_{z=z_f} \in (-\infty, 0)] = 0 \quad (23)$$

where \bar{v} and σ_v = mean and standard deviation of v , respectively, and are expressed as

$$\bar{v}_{z=z_f} = \ln\left[\frac{\bar{u}}{\sqrt{1+(\sigma_u/\bar{u})^2}}\right]_{z=z_f} \quad (24)$$

$$\sigma_v^2|_{z=z_f} = \ln\left[1+\left(\frac{\sigma_u}{\bar{u}}\right)^2\right]_{z=z_f} \quad (25)$$

In rolling mode, the probability of sediment entrainment is

$$P_R = P(\mathcal{E}_R < u_{z=z_f} < \mathcal{E}_S) = P(\ln \mathcal{E}_R < v_{z=z_f} < \ln \mathcal{E}_S)$$

$$\begin{aligned} &= \left[\int_{-\infty}^{\ln \mathcal{E}_S} f_v(v) dv - \int_{-\infty}^{\ln \mathcal{E}_R} f_v(v) dv \right]_{z=z_f} \\ &= \left[\int_{-\infty}^{\bar{v}} f_v(v) dv + \int_{\bar{v}}^{\ln \mathcal{E}_S} f_v(v) dv \right]_{z=z_f} \\ &\quad - \left[\int_{-\infty}^{\bar{v}} f_v(v) dv + \int_{\bar{v}}^{\ln \mathcal{E}_R} f_v(v) dv \right]_{z=z_f} \\ &= 0.5 \operatorname{erf} \left[\frac{2^{0.5} (\ln \mathcal{E}_S - \bar{v}_{z=z_f})}{\sigma_v|_{z=z_f}} \right] \\ &\quad - 0.5 \operatorname{erf} \left[\frac{2^{0.5} (\ln \mathcal{E}_R - \bar{v}_{z=z_f})}{\sigma_v|_{z=z_f}} \right] \quad (26) \end{aligned}$$

Introducing the following approximation of the error function:

$$\operatorname{erf}\left(\frac{y}{2^{0.5}}\right) = \frac{y}{|y|} \sqrt{1 - \exp\left(-\frac{2y^2}{\pi}\right)} \quad (27)$$

Equation 26 becomes

$$\begin{aligned} P_R &= 0.5 \frac{\ln \mathcal{E}_S - \bar{v}_{z=z_f}}{|\ln \mathcal{E}_S - \bar{v}_{z=z_f}|} \sqrt{1 - \exp\left[-\frac{2(\ln \mathcal{E}_S - \bar{v}_{z=z_f})^2}{\pi \sigma_v^2|_{z=z_f}}\right]} \\ &\quad - 0.5 \frac{\ln \mathcal{E}_R - \bar{v}_{z=z_f}}{|\ln \mathcal{E}_R - \bar{v}_{z=z_f}|} \sqrt{1 - \exp\left[-\frac{2(\ln \mathcal{E}_R - \bar{v}_{z=z_f})^2}{\pi \sigma_v^2|_{z=z_f}}\right]} \quad (28) \end{aligned}$$

In sliding mode, the probability of sediment entrainment is

$$P_S = P(\mathcal{E}_S < u_{z=z_f} < \mathcal{E}_L) = P(\ln \mathcal{E}_S < v_{z=z_f} < \ln \mathcal{E}_L)$$

$$\begin{aligned} &= \left[\int_{-\infty}^{\ln \mathcal{E}_L} f_v(v) dv - \int_{-\infty}^{\ln \mathcal{E}_S} f_v(v) dv \right]_{z=z_f} \\ &= \left[\int_{-\infty}^{\bar{v}} f_v(v) dv + \int_{\bar{v}}^{\ln \mathcal{E}_L} f_v(v) dv \right]_{z=z_f} \\ &\quad - \left[\int_{-\infty}^{\bar{v}} f_v(v) dv + \int_{\bar{v}}^{\ln \mathcal{E}_S} f_v(v) dv \right]_{z=z_f} \\ &= 0.5 \frac{\ln \mathcal{E}_L - \bar{v}_{z=z_f}}{|\ln \mathcal{E}_L - \bar{v}_{z=z_f}|} \sqrt{1 - \exp\left[-\frac{2(\ln \mathcal{E}_L - \bar{v}_{z=z_f})^2}{\pi \sigma_v^2|_{z=z_f}}\right]} \\ &\quad - 0.5 \frac{\ln \mathcal{E}_S - \bar{v}_{z=z_f}}{|\ln \mathcal{E}_S - \bar{v}_{z=z_f}|} \sqrt{1 - \exp\left[-\frac{2(\ln \mathcal{E}_S - \bar{v}_{z=z_f})^2}{\pi \sigma_v^2|_{z=z_f}}\right]} \quad (29) \end{aligned}$$

On the other hand, in lifting mode, the probability of sediment entrainment is

$$P_L = P(u_{z=z_f} > \mathcal{E}_L) = P(v_{z=z_f} > \ln \mathcal{E}_L)$$

$$\begin{aligned} &= 1 - \left[\int_{-\infty}^{\bar{v}} f_v(v) dv + \int_{\bar{v}}^{\ln \mathcal{E}_L} f_v(v) dv \right]_{z=z_f} \\ &= 0.5 - 0.5 \frac{\ln \mathcal{E}_L - \bar{v}_{z=z_f}}{|\ln \mathcal{E}_L - \bar{v}_{z=z_f}|} \\ &\quad \times \sqrt{1 - \exp\left[-\frac{2(\ln \mathcal{E}_L - \bar{v}_{z=z_f})^2}{\pi \sigma_v^2|_{z=z_f}}\right]} \quad (30) \end{aligned}$$

Using Equations 12–14, 24 and 25 into Equations 28–30 yields

$$\begin{aligned} P_R &= 0.5 \frac{\ln[G_S(1+\lambda^2)/(u_{z=z_f}^{+2} \Theta)]}{|\ln[G_S(1+\lambda^2)/(u_{z=z_f}^{+2} \Theta)]|} \\ &\quad \times \sqrt{1 - \exp\left\{-\frac{0.5 \cdot \ln^2[G_S(1+\lambda^2)/(u_{z=z_f}^{+2} \Theta)]}{\pi \cdot \ln^2(1+\lambda^2)}\right\}} \\ &\quad - 0.5 \frac{\ln[G_R(1+\lambda^2)/(u_{z=z_f}^{+2} \Theta)]}{|\ln[G_R(1+\lambda^2)/(u_{z=z_f}^{+2} \Theta)]|} \\ &\quad \times \sqrt{1 - \exp\left\{-\frac{0.5 \cdot \ln^2[G_R(1+\lambda^2)/(u_{z=z_f}^{+2} \Theta)]}{\pi \cdot \ln^2(1+\lambda^2)}\right\}} \quad (31) \end{aligned}$$

$$\begin{aligned}
P_S &= 0.5 \frac{\ln[G_L(1+\lambda^2)/(u_{z=\hat{z}_f}^{+2} \Theta)]}{|\ln[G_L(1+\lambda^2)/(u_{z=\hat{z}_f}^{+2} \Theta)]|} \\
&\times \sqrt{1 - \exp\left\{-\frac{0.5}{\pi} \cdot \frac{\ln^2[G_L(1+\lambda^2)/(u_{z=\hat{z}_f}^{+2} \Theta)]}{\ln^2(1+\lambda^2)}\right\}} \\
&- 0.5 \frac{\ln[G_S(1+\lambda^2)/(u_{z=\hat{z}_f}^{+2} \Theta)]}{|\ln[G_S(1+\lambda^2)/(u_{z=\hat{z}_f}^{+2} \Theta)]|} \\
&\times \sqrt{1 - \exp\left\{-\frac{0.5}{\pi} \cdot \frac{\ln^2[G_S(1+\lambda^2)/(u_{z=\hat{z}_f}^{+2} \Theta)]}{\ln^2(1+\lambda^2)}\right\}} \quad (32)
\end{aligned}$$

$$\begin{aligned}
P_L &= 0.5 - 0.5 \frac{\ln[G_L(1+\lambda^2)/(u_{z=\hat{z}_f}^{+2} \Theta)]}{|\ln[G_L(1+\lambda^2)/(u_{z=\hat{z}_f}^{+2} \Theta)]|} \\
&\times \sqrt{1 - \exp\left\{-\frac{0.5}{\pi} \cdot \frac{\ln^2[G_L(1+\lambda^2)/(u_{z=\hat{z}_f}^{+2} \Theta)]}{\ln^2(1+\lambda^2)}\right\}} \quad (33)
\end{aligned}$$

where $\lambda = (\sigma_u^+ / u^+)_{z=\hat{z}_f}$; and G_R , G_S and G_L are

$$G_R = \frac{\pi \hat{L}_x}{3 \hat{A}_f (C_D \hat{L}_z + C_L \hat{L}_x)}; \quad G_S = \frac{\pi \tan \phi}{3 \hat{A}_f (C_D + C_L \tan \phi)};$$

$$\text{and } G_L = \frac{\pi}{3 \hat{A}_f C_L}.$$

3 BEDLOAD FLUX IN THE CONTINUUM SCALE

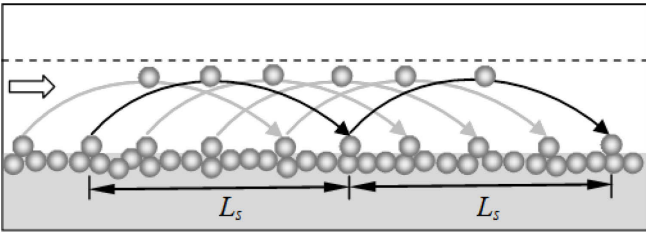


Figure 5. Schematic of bedload flux in a continuum scale.

According to the bedload hypothesis of Einstein (1950), the effective mode of grain motion as bedload transport is saltation, where the sediment grains exhibit a series of brief jumps having an approximately same step length (an average step length L_s) within the bedload layer (Fig. 5). In a continuum scale, the bedload flux can therefore be obtained by means of the entrainment probability in lifting mode obtained at the grain scale. The number of sediment grains N per unit width entrained during a short time period dt into the bedload layer is therefore given by

$$N = \frac{4A_b}{\pi D^2} P_L C_b \quad (34)$$

where A_b = bed surface area having a unit width ($= 1 \times L_s$); and C_b = bedload concentration.

The average step length L_s increases with an increase in time-averaged lift force \bar{F}_L , but it decreases with submerged weight F_G of grains. Thus, the following relation of sediment entrainment as bedload is written:

$$\frac{L_s}{D} \sim \frac{\bar{F}_L}{F_G} = \frac{K_1}{\Psi_B} C_L (u^{+2} + \sigma_u^{+2})_{z=\hat{z}_f} \quad (35)$$

where K_1 = proportionality constant including the added mass coefficient; and Ψ_B = flow intensity function ($= \Theta^{-1}$).

Hu & Hui (1996) stated that the lifting velocity of a grain can be approximated by a linear relationship of shear velocity u^* . Thus, the time period dt for a sediment grain to be entrained from the bed is inversely proportional to u^* (Wang et al., 2008). Therefore, the time period dt is given by

$$dt \sim \frac{D}{u^*} = K_2 \frac{D}{u^*} \quad (36)$$

where K_2 = proportionality constant.

The bedload flux g_B in weight per unit time and width is thus expressed as

$$g_B = \frac{N}{dt} \rho_s g \frac{\pi D^3}{6} \quad (37)$$

Inserting Equations 34–36 into Equation 37, the nondimensional bedload flux Φ_B , called bedload flux function, is obtained as

$$\begin{aligned}
\Phi_B &= \frac{g_B}{\rho_s g (\Delta g D^3)^{0.5}} \\
&= K_3 C_b C_L P_L (u^{+2} + \sigma_u^{+2})_{z=\hat{z}_f} \Psi_B^{-1.5} \quad (38)
\end{aligned}$$

where K_3 = coefficient [$= 2K_1/(3K_2)$].

To solve Equation 38, the values of C_b and K_3 are essential. In this study, $C_b = 0.65$ is considered as the maximum bedload concentration, as obtained by van Rijn (1981). However, the value of K_3 determined from the experimental data of Gilbert (1914), Meyer-Peter et al. (1934), Einstein (1942), Meyer-Peter & Müller (1948), Smart (1984), Wilcock (1988) and Chein & Wan (1999) was 4.5, which is used in this study.

4 COMPUTATIONAL STEPS

The computational steps involved to determine the entrainment thresholds and corresponding probabilities (P_R , P_S and P_L) in different modes and the bedload flux function (Φ_B) are as follows:

(1) For a given ϕ , determine \hat{d} from Equation (5) or vice-versa.

- (2) Determine $\hat{\delta}$ and \hat{A}_f from Equations (2) and (10), respectively.
- (3) For a given R^* , identify the flow regime: Smooth flow if $R^* \leq 3$, transitional flow if $3 < R^* < 70$ and rough flow if $R^* \geq 70$.
- (4) Determine \hat{z}_f from Equation (9), using the u^+ from Equation (20) for smooth and transitional flow regimes and Equation (21) for rough flow regime.
- (5) Determine $u_{z=\hat{z}_f}^+$ from Equation (20) or (21).
- (6) Determine $\sigma_u^+|_{z=\hat{z}_f}$ from Equation (22).
- (7) Determine \hat{L}_x and \hat{L}_z from Equations (18) and (19), respectively.
- (8) Determine C_D from $C_D = A_1 + A_2 R^{-1} + A_3 R^{-2}$, with $R = R^* u_{z=\hat{z}_f}^+ / k_s$.
- (9) Determine Θ_c from Equations (15)–(17).
- (10) For a given median grain size D of sediment, determine the grain function $S^* = D(\Delta g D)^{0.5} / \nu$.
- (11) Determine Θ from $\Theta = R^2 / (S^2 k_s^2)$.
- (12) Determine P_R , P_S and P_L from Equations (31)–(33), respectively.
- (13) Determine Φ_B from Equation (38).

5 RESULTS AND DISCUSSION

To show the results, the characteristic values of mass density of sediment ρ_p , mass density of fluid ρ_f and coefficient of kinematic viscosity of fluid ν are taken as 2650 kg m^{-3} , 10^3 kg m^{-3} and $10^{-6} \text{ m}^2 \text{ s}^{-1}$, respectively, for a bed of uniform sediment ($\hat{d} = 1$).

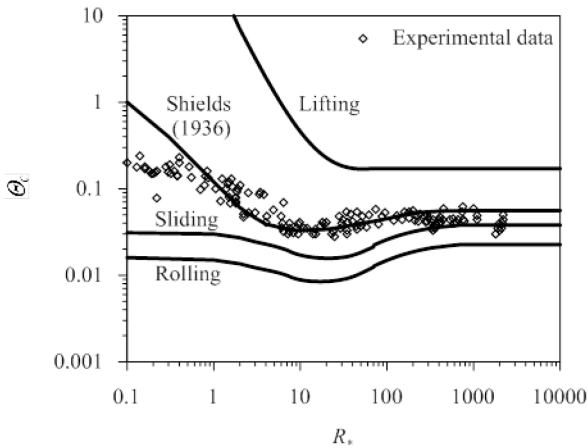


Figure 6. Threshold Shields function Θ_c versus shear Reynolds number R^* in rolling, sliding and lifting modes.

Figure 6 shows the curves of threshold Shields function Θ_c versus shear Reynolds number R^* in rolling, sliding and lifting modes. The Shields curve (1936) and the experimental data of several investigators (Gilbert, 1914; Casey, 1935; Kramer, 1935; Shields, 1936; USWES, 1936; White, 1940; Vanoni, 1946; Meyer-Peter & Müller, 1948; Iwagaki, 1956; Neill, 1967; Grass, 1970; White, 1970; Karahan, 1975; Mantz, 1977; Yalin & Karahan, 1979) are also overlapped. From $\Theta_c(R^*)$ -curves and the experi-

mental data shown in Figure 6, it is obvious that the entrainment threshold mainly belongs between the sliding and lifting modes. This study shows that the sliding threshold is the transition from rolling to lifting threshold. It is evident that the threshold Shields function Θ_c in rolling mode diminishes with an increase in R^* becoming a minimum as $\Theta_c = 0.008$ at $R^* = 20$ and then gradually increases to reach a constant value as $\Theta_c = 0.023$ at $R^* \geq 700$. The trend of sliding threshold curve is similar to that of rolling threshold curve. The Θ_c in sliding mode diminishes with an increase in R^* becoming a minimum as $\Theta_c = 0.016$ at $R^* = 20$ and then gradually increases to reach a constant value as $\Theta_c = 0.038$ for $R^* \geq 700$. On the other hand, the Θ_c in lifting mode decreases with an increase in R^* reaching a constant value as $\Theta_c = 0.171$ for $R^* > 70$.

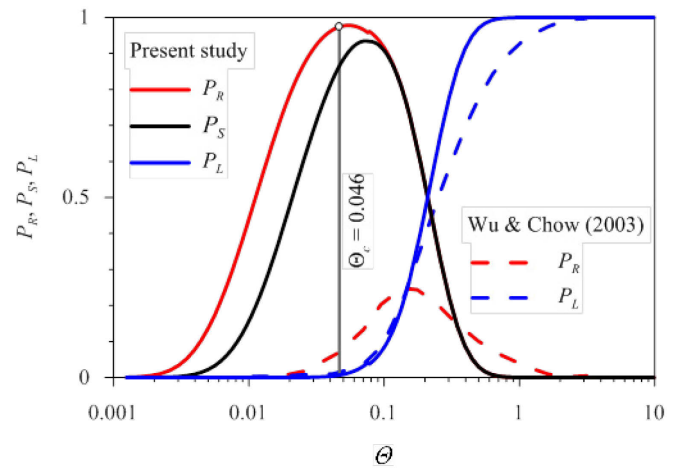


Figure 7. Variations of entrainment probabilities in rolling P_R , sliding P_S and lifting P_L modes with Shields function Θ .

Figure 7 shows the variations of entrainment probabilities in rolling P_R , sliding P_S and lifting P_L modes with Shields function Θ for a grain function $S^* = 127.2$ (that is, $D = 1 \text{ mm}$). The rolling probability P_R , at the initial stage, increases with an increase in Θ attaining a maximum as $P_R = 0.97$ at $\Theta = 0.052$ and then diminishes with Θ . The sliding probability P_S follows the similar trend to the rolling probability reaching a maximum as $P_S = 0.94$ at $\Theta = 0.072$. On the other hand, the lifting probability P_L increases with an increase in Θ attaining a maximum as $P_L = 1$ at $\Theta = 0.9$. It is evident that for the lower values of Θ ($\Theta < 0.2$), the rolling and sliding are the prevailing modes of sediment entrainment, while for the higher values of Θ ($\Theta > 0.2$), sediment grains mainly entrain in a lifting mode performing saltation. These findings are in agreement with the experimental observations of Hu & Guo (2011). They observed that the rolling and saltating (lifting) modes are prevailing for $\Theta < 0.1$ and $\Theta > 0.2$, respectively. The curves of Wu & Chow (2003) are also furnished in Figure 7 for the comparison. However, Wu & Chow (2003) abandoned the sliding mode of entrainment in their analysis. The $P_R(\Theta)$ - and $P_L(\Theta)$ -curve of this study

show a major departure from those obtained by Wu & Chow (2003). It may be noted that the $P_R(\theta)$ -curve of Wu & Chow (2003) is not well supported by the experimental findings of Hu & Guo (2011) for rolling mode ($\theta < 0.1$). The reason for such a departure can be explained as follows:

Wu & Chow (2003) treated the bed sediment grains as randomly arranged and therefore, the exposure of grains was treated as a random variable. As a consequence, the $P_R(\theta)$ - and $P_L(\theta)$ -curve were achieved based on the mean probabilities of grain entrainment, that is the integrated values of $P_R(\theta)$ and $P_L(\theta)$ over the entire range of grain exposure. However, this study highlights the entrainment of the exposed sediment grains over a compact granular sediment bed, because the bedload flux is obtained in saltating mode in a continuum scale from the entrainment probability of sediment grains in lifting mode obtained at the grain scale. One of the essential features of Figure 7 is that the maximum of $P_R(\theta)$ -curve nearly corresponds to $\theta_c = 0.046$, which is the threshold Shields function in rough flow (Yalin & Karahan, 1979) and interestingly, the initiation of lifting mode starts from that point ($\theta_c = 0.046$), as the $P_L(\theta)$ -curve has a threshold at $\theta_c = 0.046$. Figure 7 further shows that for $\theta > 0.1$, the $P_R(\theta)$ - and $P_S(\theta)$ -curve coincide to produce a single curve, demonstrating that for higher θ ($\theta > 0.1$), the entrainment probabilities in rolling and sliding modes are equal.

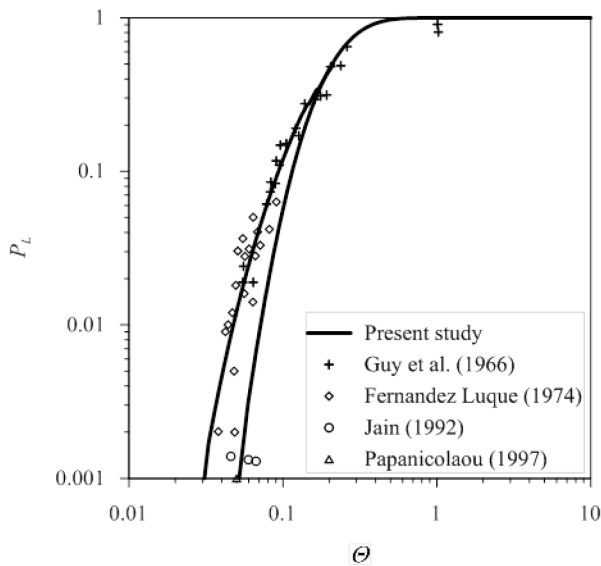


Figure 8. Variation of entrainment probability in lifting P_L mode with Shields function θ .

The variation of entrainment probability in lifting mode P_L with Shields function θ is further depicted in Figure 8. The reason to show two $P_L(\theta)$ -curves in Figure 8 is to provide the domain of the dependency of $P_L(\theta)$ on grain function S^* . The right and left bound $P_L(\theta)$ -curves correspond to the grain functions $S^* = 307$ (that is, $D = 1.8$ mm) and 91 (that is, $D = 0.8$ mm), respectively. The right and left bound

curves do not seemingly vary for $S^* > 307$ and $S^* < 91$, respectively, signifying that a dependency of $P_L(\theta)$ on S^* is predominant for $91 \leq S^* \leq 307$ (that is the zone confined to the right and left bound curves). The experimental data of Guy et al. (1966), Fernandez Luque (1974), Jain (1992) and Papanicolaou (1997) are also plotted for the comparison. Both the right and left bound $P_L(\theta)$ -curves monotonically increase approaching each other with an increase in θ and finally coincide to become a single curve for $P_L > 0.2$ ($\theta > 0.45$), where the effect of S^* on $P_L(\theta)$ is insignificant. Strictly, the left bound curve has a better agreement with the experimental data. Figure 8 shows that for a given θ , the left bound $P_L(\theta)$ -curve predicts higher P_L value than the right bound $P_L(\theta)$ -curve. This observation is evident since the entrainment probability in lifting mode for the finer grains is higher than that for the coarser ones provided that both the finer and coarser grains are subjected to the same applied bed shear stress. For $\theta = 0.046$, that is the threshold Shields function in rough flow (Yalin & Karahan, 1979), the entrainment probabilities in lifting mode obtained from the right and left bound $P_L(\theta)$ -curves of this study are 0.1 and 0.85% , respectively. It signifies that in an average, 0.48% of total bed sediment grains entrain per unit area of bed surface.

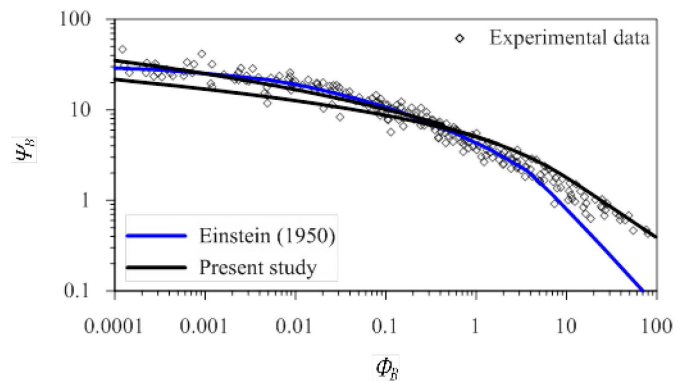


Figure 9. Variation of bedload flux function Φ_B with flow intensity function Ψ_B .

The variation of bedload flux function Φ_B with flow intensity function Ψ_B is shown in Figure 9. The experimental data of several investigators (Gilbert, 1914; Meyer-Peter et al., 1934; Einstein, 1942; Meyer-Peter & Müller, 1948; Smart, 1984; Wilcock, 1988; Chein & Wan, 1999) are also shown. The reason to show two $\Phi_B(\Psi_B)$ -curves in Figure 9 is to provide the domain of the dependency of $\Phi_B(\Psi_B)$ on grain function S^* . The upper and lower bound $\Phi_B(\Psi_B)$ -curves obtained from this study correspond to $S^* = 91$ (that is, $D = 0.8$ mm) and 1018 (that is, $D = 4$ mm), respectively (Fig. 9). The upper and lower bound curves do not seemingly vary for $S^* < 91$ and $S^* > 1018$, respectively, signifying that a dependency of $\Phi_B(\Psi_B)$ on S^* exists for $91 \leq S^* \leq 1018$ (that is the zone confined to the upper and lower bound curves). Figure 9 illustrates that Φ_B diminishes with an in-

crease in $\Psi_B (= \Theta^{-1})$, implying that the bedload flux increases with an increase in Shields function Θ . Moreover, for a given Ψ_B , the upper bound $\Phi_B(\Psi_B)$ -curve predicts a higher Φ_B than the lower bound $\Phi_B(\Psi_B)$ -curve, demonstrating that under the same applied bed shear stress, the bedload flux for the finer grains is larger than that for the coarser ones. Interestingly, for $\Psi_B < 6$, the upper and lower bound $\Phi_B(\Psi_B)$ -curves coincide to become a single curve. The comparison of $\Phi_B(\Psi_B)$ -curves of this study with the experimental data shows an acceptable agreement over a wide range of Ψ_B , although the small portion of $\Phi_B(\Psi_B)$ -curve departs marginally from the experimental data for $1 < \Psi_B < 5$. To be precise, the upper bound curve of this study has a better agreement with the experimental data. The $\Phi_B(\Psi_B)$ -curves of Einstein (1950) is further shown for the comparison. It is evident that the $\Phi_B(\Psi_B)$ -curve of Einstein (1950) departs from the experimental data for a lower Ψ_B ($\Psi_B < 2$).

6 CONCLUSIONS

A mathematical theory of sediment transport elucidating the entrainment of sediment grains from the grain scale of entrainment to the continuum scale of bedload flux for a unidirectional flow over a sediment bed is developed. The sediment grains are subjected to hydraulically smooth, transitional and rough wall-shear flows. At the grain scale, the forces acting on a spherical solitary sediment grain resting over three similar compact sediment grains are analysed to obtain the criteria for entrainment threshold in rolling, sliding and lifting modes. The time-averaged velocity laws of hydraulically smooth, transitional and rough flows are considered for the analysis, incorporating the turbulence effects. The experimental data shows that the entrainment threshold lies within the sliding and lifting modes. The entrainment probabilities in rolling, sliding and lifting modes at the grain scale are obtained by applying the log-normal probability function for the near-bed instantaneous horizontal velocity. The entrainment probabilities in rolling and sliding modes increase with an increase in Shields function to reach their individual maximum values and then they reduce. On the other hand, the entrainment probability in lifting mode increases monotonically with an increase in Shields function. The maximum value of entrainment probability in rolling mode almost corresponds to the threshold Shields function in rough flow and the initiation of entrainment probability in lifting mode corresponds to the threshold Shields function in rough flow. The variation of entrainment probability in lifting mode with Shields function reveals that the entrainment probability curves in lifting mode are confined to the right and left bound curves, corresponding to grain functions $S^* = 307$

and 91, respectively. In the continuum scale, the bedload flux is derived considering the saltation of sediment grains being the main mechanism of bedload transport. Thus, the lifting probability is relevant for the bedload transport. The variation of bedload flux function with flow intensity function indicates that the bedload flux curves are confined to the upper and lower bound curves, corresponding to $S^* = 91$ and 1018, respectively.

REFERENCES

- Abbott, J.E. & Francis, J.R.D. 1977. Saltation and suspension trajectories of solid grains in a water stream. *Philosophical Transactions of the Royal Society of London A* 284(1321): 225–254.
- Bagnold, R.A. 1956. The flow of cohesionless grains in fluids. *Philosophical Transactions of the Royal Society of London A* 249(964): 315–319.
- Best, J., Bennett, S., Bridge, J. & Leeder, M. 1997. Turbulence modulation and particle velocities over flat sand beds at low transport rates. *Journal of Hydraulic Engineering* 123(12): 1118–1129.
- Buffington, J.M. & Montgomery, D.R. 1997. A systematic analysis of eight decades of incipient motion studies, with special reference to gravel-bedded rivers. *Water Resources Research* 33(8): 1993–2029.
- Casey, H.J. 1935. Über geschiebebewegung. *Mitteilungen der Preussischen Versuchsanstalt für Wasserbau und Schiffbau*, Berlin.
- Cheng, N.S. & Chiew, Y.M. 1998. Pickup probability for sediment entrainment. *Journal of Hydraulic Engineering* 124(2): 232–235.
- Chien, N. & Wan, Z. 1999. *Mechanics of sediment transport*. Reston: American Society of Civil Engineers.
- Clifford, N.J., McClatchey, J. & French, J.R. 1991. Measurements of turbulence in the benthic boundary layer over a gravel bed and comparison between acoustic measurements and predictions of the bedload transport of marine gravels. *Sedimentology* 38(1): 161–171.
- Dey, S. 2014. *Fluvial hydrodynamics: hydrodynamic and sediment transport phenomena*. Berlin: Springer.
- Dey, S., Das, R., Gaudio, R. & Bose, S.K. 2012. Turbulence in mobile-bed streams. *Acta Geophysica* 60(6): 1547–1588.
- Dey, S., Sarkar, S. & Solari, L. 2011. Near-bed turbulence characteristics at the entrainment threshold of sediment beds. *Journal of Hydraulic Engineering* 137(9): 945–958.
- Einstein, H.A. 1942. Formulas for the transportation of bed load. *Transactions of the American Society of Civil Engineers* 107: 561–577.
- Einstein, H.A. 1950. The bed-load function for sediment transportation in open channel flows. *Technical Bulletin Number 1026*, United States Department of Agriculture, Soil Conservation Service, Washington, DC.
- Fenton, J.D. & Abbott, J.E. 1977. Initial movement of grains on a stream bed: the effect of relative protrusion. *Proceedings of the Royal Society of London A* 352(1671): 523–537.
- Fernandez Luque, R. 1974. Erosion and transport of bed-load sediment. *Ph.D. thesis*, Delft University of Technology, Meppel.
- Francis, J.R.D. 1973. Experiments on the motion of solitary grains along the bed of a water-stream. *Proceedings of the Royal Society of London A* 332(1591): 443–471.

- Garcia, M.H. 2008. *Sedimentation engineering: processes, measurements, modeling, and practice*. Reston: American Society of Civil Engineers.
- Gilbert, G.K. 1914. Transportation of debris by running water. *Professional paper number 86*, United States Geological Survey, Washington DC.
- Grass, A.J. 1970. Initial instability of fine bed sand. *Journal of the Hydraulics Division* 96(3): 619–632.
- Guy, H.P., Simons, D.B. & Richardson, E.V. 1966. Summary of alluvial channel data from flume experiments, 1956–1961. *Report 462-1*, United States geological survey water supply paper number, Washington DC.
- Heathershaw, A.D. & Thorne, P.D. 1985. Sea-bed noises reveal role of turbulent bursting phenomenon in sediment transport by tidal currents. *Nature* 316: 339–342.
- Hu, C. & Guo, Q. 2011. Near-Bed sediment concentration distribution and basic probability of sediment movement. *Journal of Hydraulic Engineering* 137(10): 269–275.
- Hu, C.H. & Hui, Y.J. 1996. Bed-load transport. I: Mechanical characteristics. *Journal of Hydraulic Engineering* 122(5): 245–254.
- Iwagaki, Y. 1956. Fundamental study on critical tractive force. *Transactions of the Japan Society of Civil Engineers* 41: 1–21.
- Jain, S. 1992. Note on lag in bedload discharge. *Journal of Hydraulic Engineering* 118(6): 904–917.
- Karahan, E. 1975. Initiation of motion for uniform and non-uniform materials. *Ph.D. thesis*, Technical University, Istanbul.
- Kline, S.J., Reynolds, W.C., Schraub, F.A. & Runstadler, P.W. 1967. The structure of turbulent boundary layers. *Journal of Fluid Mechanics* 30: 741–773.
- Kramer, H. 1935. Sand mixtures and sand movement in fluvial model. *Transactions of the American Society of Civil Engineers* 100: 798–838.
- Mantz, P.A. 1977. Incipient transport of fine grains and flakes by fluids—extended Shields diagram. *Journal of the Hydraulics Division* 103(6): 601–615.
- Meyer-Peter, E. & Müller, R. 1948. Formulas for bed-load transport. In *Proceedings of the 2nd meeting of International Association for Hydraulic Research*, Vol. 3, Stockholm: 39–64.
- Meyer-Peter, E., Favre, H. & Einstein, H.A. 1934. Neuere versuchsresultate über den geschiebtrieb. *Schweizerische Bauzeitung* 103(4): 147–150.
- Miller, M.C., McCave, I.N. & Komar, P.D. 1977. Threshold of sediment motion under unidirectional currents. *Sedimentology* 24(4): 507–527.
- Miller, R.L. & Byrne, R.J. 1966. The angle of repose for a single grain on a fixed rough bed. *Sedimentology* 6(4): 303–314.
- Morsi, S.A. & Alexander, A.J. 1972. An investigation of particle trajectories in two-phase flow systems. *Journal of Fluid Mechanics* 55: 193–208.
- Neill, C.R. 1967. Mean velocity criterion for scour of coarse uniform bed material. In *Proceedings of the 12th Congress of International Association for Hydraulic Research*, Vol. 3, Colorado: 46–54.
- Nezu, I. 1977. Turbulent structure in open channel flow. *Ph.D. thesis*, Kyoto University, Kyoto.
- Papanicolaou, A.N. 1997. The role of turbulence on the initiation of sediment motion. *Ph.D. thesis*, Virginia Institute of Technology, Virginia.
- Papanicolaou, A.N., Diplas, P., Dancy, C.L. & Balakrishnan, M. 2001. Surface roughness effects in near-bed turbulence: implications to sediment entrainment. *Journal of Engineering Mechanics* 127(3): 211–218.
- Papanicolaou, A.N., Diplas, P., Evaggelopoulos, N. & Fotopoulos, S. 2002. Stochastic incipient motion criterion for spheres under various bed packing conditions. *Journal of Hydraulic Engineering* 128(4): 369–380.
- Reichardt, H. 1951. Vollständige darstellung der turbulenten geschwindigkeitsverteilung in glatten leitungen. *Zeitschrift für Angewandte Mathematik und Mechanik* 31(7): 208–219.
- Schmeeckle, M.W. & Nelson, J.M. 2003. Direct numerical simulation of bedload transport using a local, dynamic boundary condition. *Sedimentology* 50(2): 279–301.
- Shields, A.F. 1936. Application of similarity principles and turbulence research to bed-load movement. *Mitteilungen der Preussischen Versuchsanstalt für Wasserbau und Schiffbau*, Vol. 26, Berlin: 5–24.
- Smart, G.M. 1984. Sediment transport formula for steep channels. *Journal of Hydraulic Engineering* 110(3): 267–276.
- Sutherland, A.J. 1967. Proposed mechanism for sediment entrainment by turbulent flows. *Journal of Geophysical Research* 72(4): 6183–6194.
- Tregnaghi, M., Bottacin-Busolin, A., Marion, A. & Tait, S. 2012. Stochastic determination of entrainment risk in uniformly sized sediment beds at low transport stages: 1. Theory. *Journal of Geophysical Research* 117(F04004): 1–15.
- USWES. 1936. Flume tests made to develop a synthetic sand which will not form ripples when used in movable bed models. *Technical memorandum 99-1*, United States Waterways Experiment Station, Vicksburg, Mississippi.
- van Rijn, L.C. 1981. Computation of bed-load concentration and bed-load transport. *Research report S 487-1*, Delft Hydraulics Laboratory, Delft.
- Vanoni, V.A. 1946. Transportation of suspended sediment by water. *Transactions of the American Society of Civil Engineers* 111: 67–102.
- Wang, X., Zheng, J., Danxun, L. & Qu, Z. 2008. Modification of the Einstein bed-load formula. *Journal of Hydraulic Engineering* 134(9): 1363–1369.
- White, C.M. (1940) The equilibrium of grains on the bed of a stream. *Proceedings of the Royal Society of London A* 174(958): 322–338.
- White, S.J. 1970. Plane bed thresholds of fine grained sediments. *Nature* 228(October): 152–153.
- Wiberg, P.L. & Smith, J.D. 1987. Calculations of the critical shear stress for motion of uniform and heterogeneous sediments. *Water Resources Research* 23(8): 1471–1480.
- Wilcock, P.R. 1988. Methods for estimating the critical shear stress of individual fractions in mixed-size sediment. *Water Resources Research* 24(7): 1127–1135.
- Williams, J.J., Thorne, P.D. & Heathershaw, A.D. 1989. Measurements of turbulence in the benthic boundary layer over a gravel bed. *Sedimentology* 36(6): 959–971.
- Wu, F.C. & Chou, Y.J. 2003. Rolling and lifting probabilities for sediment entrainment. *Journal of Hydraulic Engineering* 129(2): 110–119.
- Wu, F.C. & Jiang, M.R. 2007. Numerical investigation of the role of turbulent bursting in sediment entrainment. *Journal of Hydraulic Engineering* 133(3): 329–334.
- Wu, F.C. & Lin, Y.C. 2002. Pickup probability of sediment under log-normal velocity distribution. *Journal of Hydraulic Engineering* 128(4): 438–442.
- Wu, F.C. & Yang, K.H. 2004. A stochastic partial transport model for mixed-size sediment: application to assessment of fractional mobility. *Water Resources Research* 40(W04501): 1–18.

- Yalin, M.S. & Karahan, E. 1979. Inception of sediment transport. *Journal of the Hydraulics Division* 105(11): 1433–1443.
- Zanke, U.C.E. 2003. On the influence of turbulence on the initiation of sediment motion. *International Journal of Sediment Research* 18(1): 17–31.